Astronomy & Astrophysics manuscript no. output
September 27, 2022

ZZ Ceti stars of the southern ecliptic hemisphere re-observed by TESS

Zs. Bognár[1,2,3,⋆], and Á. Sódor[1,2,3]

[1] Konkoly Observatory, Eötvös Loránd Research Network (ELKH), Research Centre for Astronomy and Earth Sciences, Konkoly Thege Miklós út 15-17, H–1121, Budapest, Hungary
[2] MTA CSFK Lendület Near-Field Cosmology Research Group
[3] MTA Centre of Excellence

ABSTRACT

Context. In 2020, a publication presented the first-light results on 18 known ZZ Ceti stars observed by the TESS space telescope during the first survey observations of the southern ecliptic hemisphere. However, in the meantime, new measurements have became available from this field, in many cases with the new, 20 s ultra-short cadence mode.
Aims. We investigated the similarities and differences of the pulsational behaviour of the observed stars between the two observational seasons, and searched for newly detected pulsation modes for asteroseismology.
Methods. We performed Fourier analyses of the light curves by the standard pre-whitening process, and compared the resulting sets of frequencies with those obtained by the earlier data.
Results. We detected several new possible pulsation modes of the studied pulsators. In the case of HE 0532-5605, we found a similar brightening phase as the one was presented in the 2020 first-light paper, that is, the phenomenon was repeated. Therefore, HE 0532-5605 is a new outbursting DAV star with high probability. We also detected a lower-amplitude brightening phase in the star WD J0925+0509. However, this case has proven to be the result of the passage of a Solar System object in the foreground.

Key words. techniques: photometric – stars: oscillations – white dwarfs

1. Introduction

This paper focuses on the study of ZZ Ceti stars observed by the Transiting Exoplanet Survey Satellite (TESS; Ricker et al. 2015). TESS was launched on 18 April 2018, and during its two-year primary mission, it provided 30-minute (long) cadence full-frame images from almost the entire sky, and 120-second (short) cadence observations on selected targets. The main goal of the mission is to find exoplanets at bright nearby stars with the transit method, but the time sampling of the observations also allow the examination of any kind of light variations of the stars in the observed fields. Due to their short periods, only the short cadence mode is suitable for studying the light variations of compact pulsators. The first-light papers of the TESS Asteroseismic Science Consortium (TASC) Compact Pulsators Working Group (WG#8), presented e.g. by Bell et al. (2019), Charpinet et al. (2019), and Bognár et al. (2020), clearly demonstrated the suitability of the TESS measurements for compact pulsators. Moreover, TESS observations significantly raised (by about 20 per cent) the number of known DAV stars (Romero et al. 2022).

Fortunately, the mission was not ended after two years, but an Extended Mission was approved for the 2020–2022 years, with some modifications, e.g. in the cadence of the observations: the full-frame image cadence was reduced to 10 minutes, while new, 20-second ultra-short cadence mode measurements also became available, which are great improvements, considering the demands of the compact pulsator studies.

ZZ Ceti or DAV stars are short-period ($P \sim 100 - 1500$ s), low-amplitude ($A \sim 0.1\%$) variables, which requires precise and short-exposure-time measurements both from the ground and from space. Their atmospheres are dominated by hydrogen, and they form the most populous group of pulsating white dwarf stars, laying in the 10 500–13 000 K effective temperature range. Their pulsation modes are low-spherical-degree ($\ell = 1$ and 2), and low-to-mid radial-order g-modes. The $\kappa - \gamma$ mechanism (Dolez & Vauclair 1981; Winget et al. 1982) in combination with the convective driving mechanism (Brickhill 1991; Goldreich & Wu 1999) is responsible for the excitation of the observed pulsations.

Despite the relatively narrow instability strip of the DAV stars, they can show a large variety of pulsational properties evolving from the hot (blue) to the cool (red) edge of the instability domain. Hotter DAVs show fewer and lower-amplitude pulsation modes than the cooler ones, with more and larger-amplitude frequencies. Furthermore, in this latter case, above about 800 s in period, we usually do not detect one single peak at a given frequency in the Fourier transform of the light curve, but a large number of peaks under a broad envelope, which reminds to stochastically driven oscillations. For a detailed description of the DAV instability strip and this interesting phenomenon based on observations with the Kepler space telescope, we refer the reader to the paper of Hermes et al. (2017). For reviews of the theoretical and observational aspects of studies of white dwarf pulsators, we also recommend to read the papers of Winget & Kepler (2008), Fontaine & Brassard (2008), Althaus et al. (2010), Córsico et al. (2019), and Córsico (2020).

We also mention the so-called outburst phenomena in cool DAV stars, which appears as an increase in the stellar flux of ZZ Ceti stars close to the red edge of the instability strip. These outburst events were discovered by the measurements of the Ke-

⋆ e-mail: bognar.zsofia@csfk.org

pler space telescope. Such phenomenon suggests that the average brightness of the star increases relatively fast (about an hour) with at least several per cent, and remains in this state for several of hours or even longer, sometimes even more than a day. After that, the stellar brightness decreases to the initial value, then the outburst event repeats after several days or weeks. The duration and occurrence of these events is irregular and unpredictable. For further details and references, see the proceedings of Bell et al. (2017).

This paper is the continuation of our work published in 2020 (Bognár et al. 2020, hereafter P01). We detail the main goals of the present work and some points about the light curve reduction process in Sect. 2. Sect. 3 presents the results on the light curve analyses. Finally, the summary and conclusions are presented in Sect. 4.

2. TESS observations in ultra-short cadence mode

In P01, we presented the results of the light curve analyses of 18 previously known ZZ Ceti stars, observed by TESS during the first survey of the southern ecliptic hemisphere. As TESS returned to these fields performing further observing runs, we now have a unique opportunity to check changes in the pulsational behaviour of these stars between the two observing runs. Moreover, this time TESS observed almost all of our targets in ultra-short cadence mode with 20 s exposure times, which helps distinguishing real pulsational frequencies from their Nyquist aliases. In this work, we analyse the ultra-short cadence data.

However, there are some differences between the targets presented in this paper and in P01. Because TESS did not return to the exact positions in the second run on the southern ecliptic hemisphere, TESS did not observe HS 0507+0434B, which was found to be a variable in P01. New observations of three non-variable (NOV) objects, MCT 2148-2911, WD 0108-001, and KUV 03442+0719 are also missing. On the other hand, we also found one new pulsator: HS 1013+0321 was a NOV star according to our previous analysis, while the new observations revealed pulsation frequencies reported earlier in the literature.

Without giving any details on the light-variation analyses with negative outcome, we mention that the following five NOV stars from P01 were also found to be non-variable based on the new TESS data: HE 0031-5525, EC 00497-4723, MCT 0016-2553, HS 0253+0655, and EC 11266-2217.

Therefore, we present the analyses of altogether nine ZZ Ceti stars below. We listed them and the log of observations in Table 1.

We processed the data a similar way as in P01. We downloaded the light curves from the *Mikulski Archive for Space Telescopes* (MAST), and extracted the PDCSAP fluxes provided by the pre-search data conditioning pipeline (Jenkins et al. 2016) from the fits files. It is important to mention, that this pipeline corrects the flux for each target to account for crowding from other stars. We then corrected the light curves for long-term systematics and outlier data points. Considering the trends on much longer time scales than the pulsations, at first, we divided the time strings into segments. These segments contain gaps no longer than 0.5 d. Then, we separately fitted and subtracted cubic splines from each segment. We used one knot point for every 1000 points to define the splines. Finally, we omitted the obvious outliers. The above corrections did not affect the frequency domain of the short-period white dwarf pulsations.

3. Light curve analysis

We analysed the measurements with the command-line light curve fitting program LCfit developed by Á. Sódor (Sodor 2012). Utilising an implementation of the Levenberg-Marquardt least-squares fitting algorithm, LCfit is capable of linear (amplitudes and phases) and nonlinear (amplitudes, phases and frequencies) least-squares fittings. The program also can handle unequally spaced measurements, and data sets with gaps inside.

We chose the detection limit to be at 0.1 per cent false alarm probability (FAP), just as we did in P01. This means, that there is a 99.9 per cent chance that a peak reaching this limit is not just a result of random fluctuations due to the noise. We calculated the 0.1% FAP threshold the same way we described in P01, which refers to the work of Zong et al. (2016).

In the following sections, we summarise our findings on the different stars, including a comparison between the light curve analysis results of the new and the previous observations presented in P01. We do not give as detailed description on the results of the former ground-based observations as we did in P01; we refer to our previous paper instead.

3.1. Ross 548

Ross 548 (TIC 029854433 = ZZ Ceti, $\alpha_{2000} = 01^{\rm h}36^{\rm m}14^{\rm s}$, $\delta_{2000} = -11^{\rm d}20^{\rm m}33^{\rm s}$) is the namesake of the ZZ Ceti or DAV class of pulsating white dwarf stars.

3.1.1. New TESS observations

TESS observed Ross 548 in sector 30 with the ultra-short cadence 20 s mode. Unlike in the former 120 s TESS observations, there is no Nyquist-alias problem in this new data set, thus direct determination of the frequencies was feasible. We can clearly detect the four highest-amplitude frequencies, but we did not find further modes reported by Giammichele et al. (2015). Figure 1 shows the Fourier transform (FT) of the ultra-short cadence TESS light curve. In Table 2, we summarise the findings on both the new TESS observations, together with the amplitudes resulting from ground-based measurements. We also listed the predicted TESS amplitudes calculated from the weighted mean amplitudes of the ground-based observations (see table 3 and eq. 1 in P01 for more details).

As Table 2 shows, we obtained close agreement with the ultra-short cadence mode amplitudes and the predicted amplitudes calculated from the weighted means of ground-based measurements. Furthermore, we can fine-tune our amplitude predictions with more sophisticated effective temperature determinations by e.g. high-resolution optical spectroscopic observations.

3.2. EC 23487-2424

EC 23487-2424 (TIC 033986466, $\alpha_{2000} = 23^{\rm h}51^{\rm m}22^{\rm s}$, $\delta_{2000} = -24^{\rm d}08^{\rm m}17^{\rm s}$) was discovered by Stobie et al. (1993), who found that it shows a complex frequency structure with closely spaced frequencies and harmonics.

The previous TESS observations revealed the stochastic nature of the long-period modes in accordance with the results of Hermes et al. (2017). We also detected possible rotationally split frequencies and presented the corresponding rotation periods in P01.

Table 1. Journal of observations of the targets showing light variations in the new TESS data sets. Data were collected in many cases in 20 and 120 s cadence modes, respectively, but here we list the information only on the ultra-short cadence mode, since these are the data analysed in this work. N is the number of data points after cleaning the light curve, δT is the length of the data sets including gaps, and *Sect.* is the serial number of the sector(s) in which the star was observed. The start time in BJD is the time of the first data point in the data set. The *CROWDSAP* keyword represents the ratio of the target flux to the total flux in the TESS aperture.

Object	TIC	Start time (BJD-2 457 000)	N	δT (d)	G mag	Sect.	CROWDSAP	0.1% FAP (mma)
Ross 548	029854433	2115.890	95 196	25.7	14.2	30	0.98	0.9
EC 23487-2424	033986466	2088.244	87 877	24.2	15.4	29	0.97	2.6
BPM 31594	101014997	2115.887	198 676	54.1	15.1	30–31	0.90	1.4
BPM 30551	102048288	2088.243	79 831	23.3	15.5	29	0.96	2.8
MCT 0145-2211	164772507	2115.890	99 835	26.0	15.2	30	0.96	2.6
L 19-2	262872628	2333.857	225 422	55.9	13.4	38–39	0.78	0.4
HS 1013+0321	277747736	2255.806	273 927	322.9	15.7	35,45–46	0.96	2.5
WD J0925+0509	290653324	2255.885	267 087	322.8	15.3	35,45–46	0.51	1.88
HE 0532-5605	382303117	2088.239	909 194	301.5	15.4	29–31,33–39	0.73	1.52

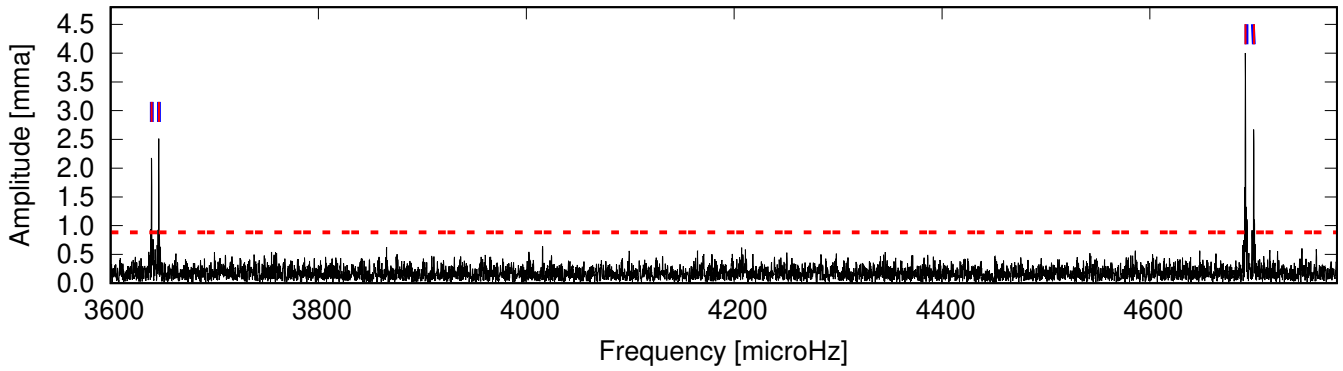

Fig. 1. Fourier transform of ultra-short cadence mode light curve of Ross 548. We mark the frequencies detected in the previous TESS season with blue lines, red lines denote the newly found frequencies, while the red dashed line corresponds to the 0.1% FAP significance level.

Table 2. Frequencies, periods, and amplitudes determined from the new, 20 s cadence mode TESS observations. For comparison, we also list the predicted amplitudes in the TESS band pass, and finally, the weighted mean amplitudes from ground-based measurements.

	Frequency [μHz]	Period [s]	Ampl. [mma]	TESS pred. ampl. 825 nm [mma]	Weighted mean ampl. [mma]
f_1	4691.908(10)	213.1329	3.98(24)	4.34	6.86(4)
f_2	4699.977(00)	212.7670	2.39(15)	2.71	4.28(4)
f_3	3646.315(16)	274.2495	2.56(22)	2.79	4.41(4)
f_4	3639.328(17)	274.7760	2.18(22)	2.01	3.17(4)

3.2.1. New TESS observations

We detected 14 frequencies above the detection limit in the light curve of the star obtained in 20 s cadence mode. For completeness, we summarise our findings together with the results of the previous observations presented in P01 in Table 3.

As Table 3 shows, the ultra-short cadence data set revealed new pulsation-frequency components. We also can notice the presence of closely spaced frequencies, which might be the results of short-term amplitude/phase/frequency variations above $\sim$ 700 s. This is practically consistent with the findings of Hermes et al. (2017), predicting stochastic behaviour of the periods above $\sim$ 800 s. Comparing the frequency contents of the EC 23487-2424 data sets obtained at different times, it is indeed obvious that amplitude variations occur between the epochs.

3.3. BPM 31594

BPM 31594 (TIC 101014997, $\alpha_{2000} = 03^{\rm h}43^{\rm m}29^{\rm s}$, $\delta_{2000} = -45^{\rm d}49^{\rm m}04^{\rm s}$) is known as a pulsator with a few independent modes, but showing several additional peaks: combination frequencies, near-subharmonic peaks, and frequencies emerging as a result of rotational frequency splitting. Amplitude variations from season to season are also known at some frequencies.

3.3.1. New TESS observations

Combining data from sectors 30 and 31, we found 43 significant peaks. However, these frequencies are not all independent pulsational modes, but several of them form frequency groups, indicating short-term amplitude/phase/frequency variations, or maybe instrumental effects. In Table 4, we summarise our findings listing the frequencies presented in P01, too. Fig. 3 shows the Fourier transform of the ultra-short cadence light curve of BPM 31594, in which we marked the new frequencies as well as the location of peaks identified in P01.

The dominant peak is at 1618.4 μHz, in agreement with the results of the previous observations. This peak and its first harmonic are also central components of two triplets with $\sim$ 13 μHz

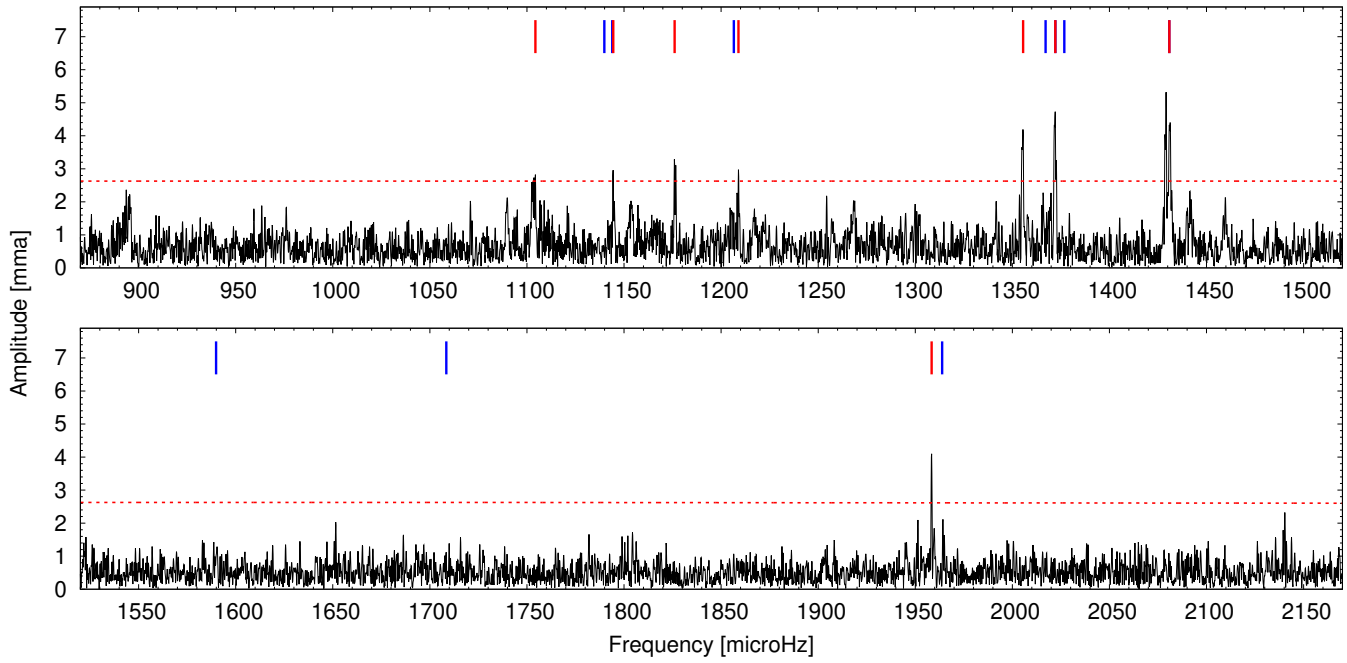

Fig. 2. Fourier transform of ultra-short cadence mode light curve of EC 23487-2424. Blue lines mark the frequencies detected in the previous TESS season (see P01), red lines denote the newly found frequencies, while the red dashed line corresponds to the 0.1% FAP significance level.

Table 3. This work: results of the fit of the EC 23487-2424 data set with 14 frequencies derived by the ultra-short cadence mode TESS observations. The frequencies in parentheses are closely spaced peaks to the larger amplitude ones, and may not represent independent pulsational frequencies. The errors are formal uncertainties. P01 frequencies: the results of Lorentzian fits are marked with asterisk (*). We also presented a possible frequency identification in column 4. In the case of the supposed rotationally split frequencies, we mark the possible azimuthal order values.

This work				P01 – Bognár et al. (2020)		
Frequency [μHz]	Period [s]	Ampl. [mma]		Frequency [μHz]	Period [s]	Ampl. [mma]
(1103.005(39)	906.615	2.65(45))				
1104.293(37)	905.557	2.84(45)	f_1			
			$f_2^{-1/0}$	1139.799(34)	877.348	3.30(49)
1144.365(35)	873.847	3.00(45)	$f_2^{0/+1}$	1144.67(35)*	873.614	1.61(30)
1175.997(31)	850.342	3.31(45)	f_3			
1208.947(35)	827.166	2.99(45)	f_4	1206.495(39)*	828.847	2.41(05)
(1355.178(30)	737.910	3.52(46))				
1355.546(26)	737.710	4.06(46)	f_5			
			f_6^{-1}	1367.082(17)	731.485	6.65(49)
(1371.708(24)	729.018	4.30(46))				
1372.103(22)	728.808	4.67(46)	f_6^{0}	1372.116(35)	728.802	3.15(49)
			f_6^{+1}	1376.720(39)	726.364	2.81(49)
(1428.764(30)	699.906	3.51(47))				
(1429.206(20)	699.689	5.32(47))				
1430.753(33)	698.933	3.15(46)	f_7	1430.780(17)	698.920	6.41(49)
(1431.165(24)	698.731	4.30(47))				
			f_8	1589.850(37)	628.990	2.96(49)
			f_9	1708.434(27)	585.331	4.05(49)
1958.384(26)	510.625	4.15(49)	f_{10}	1963.783(23)	509.221	4.88(49)

frequency separation (denoted by Δ in Table 4). Such triplets can be interpreted as rotational frequency splitting of an $\ell = 1$ mode.

There are several surprising frequencies denoted as f_x, f_y, f_w, and f_z. The origin of these peak is not clear, but it is worth to mention that the spacings between $1.54 f_4$ and f_x ($\delta f = 6.92\,\mu$Hz), and f_y and f_w ($\delta f = 6.95\,\mu$Hz), and $2.54 f_4$ and f_z ($\delta f = 5.48\,\mu$Hz) are similar. We cannot rule out that there are additional independent frequencies among these peaks. Further observations may reveal their true nature.

Note that there is another paper in preparation presenting the results of the frequency analyses of the TESS observations (Romero et al. 2022b), and also review the outcomes of asteros-

Table 4. This work: results of the fit of the BPM 31594 data set derived by the ultra-short cadence mode TESS observations. We mark with + signs where closely spaced peaks around a larger-amplitude one exist. These may not represent additional independent pulsational frequencies, thus we do not include them in this list. The errors are formal uncertainties. We also present a possible frequency identification in the 4th column.

This work				P01 – Bognár et al. (2020)		
Frequency [μHz]	Period [s]	Amplitude [mma]		Frequency [μHz]	Period [s]	Amplitude [mma]
			Δ	13.409(12)	74577	3.08(32)
871.799(18)	1147.053	1.45(24)	$0.54f_4$			
877.261(18)	1139.912	1.46(24)	f_1			
1460.726(17)	684.591	1.58(26)	f_2	1461.117(13)	684.408	2.87(32)
1548.328(7)	645.858	3.70(26)	f_3	1548.455(4)	645.805	8.47(32)
1605.950(3)$^+$	622.684	8.68(27)	$f_4 - \Delta$	1604.982(4)	623.060	8.94(32)
1618.374(1)$^+$	617.904	32.44(27)	f_4	1618.401(1)	617.894	39.37(32)
1630.778(3)$^+$	613.204	8.50(27)	$f_4 + \Delta$	1631.844(4)	612.804	10.80(32)
2483.254(4)	402.697	6.40(30)	f_x	2483.203(7)	402.706	5.06(32)
2490.171(5)$^+$	401.579	6.09(30)	$1.54f_4$	2490.147(7)	401.582	5.35(32)
3166.716(12)	315.785	2.40(32)	$f_3 + f_4$	3166.877(9)	315.769	4.05(32)
3224.310(13)	310.144	2.15(32)	$2f_4 - \Delta$			
3236.751(4)$^+$	308.952	7.21(33)	$2f_4$	3236.794(6)	308.948	6.26(32)
3245.653(6)	308.104	4.85(32)	f_y	3245.648(11)	308.105	3.41(32)
3249.136(12)$^+$	307.774	2.26(32)	$2f_4 + \Delta$			
3252.603(7)	307.446	4.24(32)	f_w	3252.590(12)	307.447	3.16(32)
4108.546(12)$^+$	243.395	2.51(35)	$2.54f_4$	4108.584(15)	243.393	2.49(32)
4114.021(12)	243.071	2.34(35)	f_z	4115.083(16)	243.009	2.41(32)
4855.098(9)$^+$	205.969	2.55(37)	$3f_4$			
5726.912(18)	174.614	1.74(39)	$3.54f_4$			

esimological investigations. They led to a slightly different conclusion considering the mode identification of the observed frequencies, and utilised those periods for asteroseismology.

3.4. BPM 30551

BPM 30551 (TIC 102048288, $\alpha_{2000} = 01^h06^m54^s$, $\delta_{2000} = -46^d08^m54^s$) shows complex pulsations in the ground-based observations.

3.4.1. New TESS observations

We analysed the ultra-short cadence data on BPM 30551 obtained in sector 29. We identified only five significant frequencies, of which two pairs form closely spaced doublets, suggesting that only three modes present in the new observations of BPM 30551. Table 5 summarises the frequencies found by the new TESS observations and also the frequencies published in P01.

This star is an excellent example for demonstrating that large amplitude variations can happen from one observing season to another: new frequencies emerge above the significance level, while the amplitude of formerly known frequencies decrease, or some of the frequencies cannot be detected at all, as Fig. 4 shows.

3.5. MCT 0145-2211

MCT 0145-2211 (TIC 164772507, $\alpha_{2000} = 01^h47^m22^s$, $\delta_{2000} = -21^d56^m51^s$) is another example on the temporal changes in the pulsation properties of cool DAVs.

3.5.1. New TESS observations

The standard pre-whitening process yielded 24 significant frequencies. However, similarly to BPM 30551, there are frequency groups of closely spaced components in the Fourier transform, suggesting that amplitude/frequency/phase variations occurred during the observations. We observe such behaviour in frequencies above 700 s. We summarise our frequency identification, together with previous results from P01 in Table 6. We note that these are the results of an automated pre-whitening process, and there can be real pulsation modes, products of rotational frequency splittings, and peaks emerging from the stochastic nature of the long-period modes.

It is conspicuous that there are no common frequencies between the two observing seasons, as if we observed two different stars. What we can find is groupings of periods around at 805 s, 795 s, 765 s, 761 s, 720 s, and 415 s. Besides these periods, there are a couple of peaks that do not belong to any groups. These peaks are promising candidates for being eigenmodes for asteroseismic investigations. Fig. 5 shows the Fourier transform of the 20 s cadence mode light curve, with the peaks found in the two different seasons marked.

3.6. L 19-2

L 19-2 (TIC 262872628, $\alpha_{2000} = 14^h33^m08^s$, $\delta_{2000} = -81^d20^m14^s$) shows a simpler and much more stable pulsational behaviour than the previous two objects (BPM 30551 and MCT 0145-2211), with only a couple of eigenmodes showing rotational splittings. In the previous TESS observations presented in P01, we found only one frequency, the Nyquist alias of the 192.6 s period.

3.6.1. New TESS observations

The analysis of the new data set on L 19-2 revealed the presence of five frequencies, listed in Table 7. For comparison, we also list the frequencies presented by Yeates et al. (2005) in Table 7. Figure 6 shows the Fourier transform of the new TESS data.

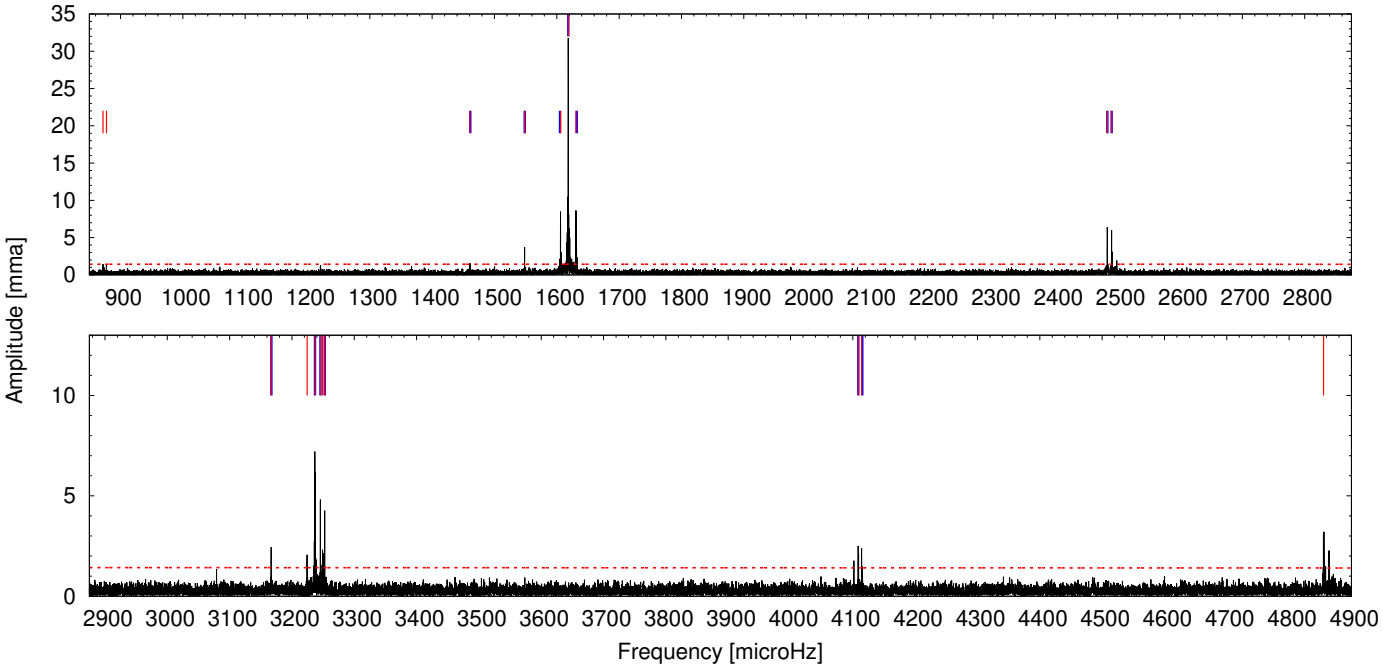

Fig. 3. Fourier transform of the ultrashort cadence TESS observations on BPM 31594. For further explanation, see the caption of Fig. 2

Table 5. This work: significant frequencies found in the sector 29 observations of BPM 30551. In the case of the P01 frequencies, they are results of Lorentzian fits to the frequency groups observed in the actual BPM 30551 data set. The central frequencies are marked with asterisks (*).

This work			P01 – Bognár et al. (2020)		
Frequency [μHz]	Period [s]	Amplitude [mma]	Frequency [μHz]	Period [s]	Amplitude [mma]
			1144.760(150)*	873.546	1.39(03)
			1204.487(021)*	830.229	3.14(02)
1208.880(33)	827.212	3.37(48)			
1209.997(27)	826.448	4.17(48)			
			1264.164(093)*	789.163	1.83(02)
1413.070(30)	707.679	3.70(49)			
1487.056(32)	672.470	3.48(49)			
1490.973(40)	670.703	2.76(49)			

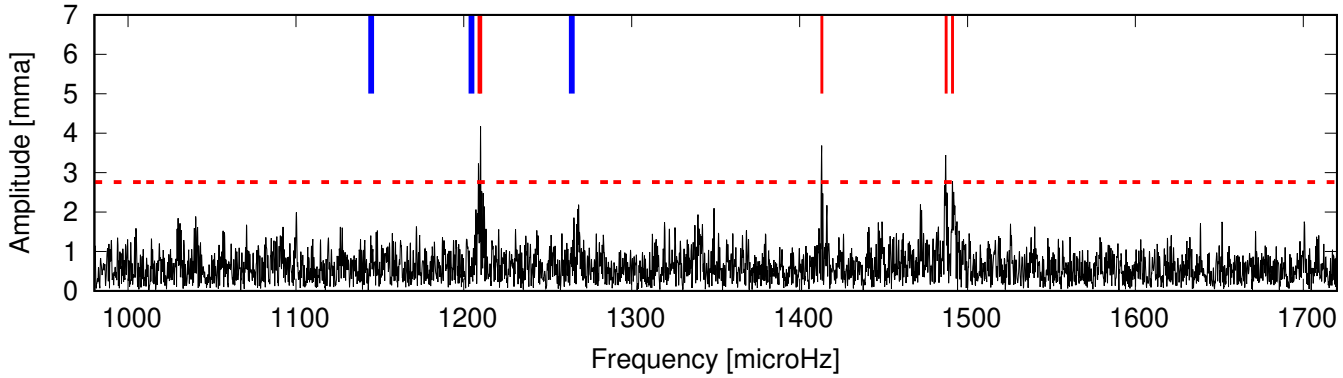

Fig. 4. Fourier transform of the ultra-short cadence TESS observations on BPM 30551. For further explanation, see the caption of Fig. 2.

3.7. HS 1013+0321

HS 1013+0321 (TIC 277747736 α_{2000} = $10^h15^m48^s$, δ_{2000} = $+03^d06^m48^s$) is a DAV star observed in P01, but those data did not show light variations (NOV in P01). Previous ground-based observations showed that this star displays stable, short-period light variations, similarly to L 19-2.

Table 6. This work: frequencies detected above the detection limit during the standard pre-whitening process. P01: also complete list of frequencies derived from the MCT 0145-2211 data set.

This work			P01 – Bognár et al. (2020)		
Frequency [μHz]	Period [s]	Amplitude [mma]	Frequency [μHz]	Period [s]	Amplitude [mma]
			955.854(044)	1046.185	3.68(53)
1240.210(34)	806.315	2.84(45)			
1241.333(29)	805.585	3.38(45)			
1243.911(35)	803.916	2.76(45)			
			1253.099(045)	798.021	3.63(1.89)
			1257.085(063)	795.491	5.29(53)
			1257.462(052)	795.252	6.40(88)
			1297.472(039)	770.730	4.13(62)
			1305.221(045)	766.154	3.72(55)
			1306.979(033)	765.123	5.21(89)
			1308.725(053)	764.103	3.18(55)
1313.363(23)	761.404	4.20(45)			
1313.666(23)	761.228	4.30(46)			
1313.991(33)	761.040	3.00(45)			
1314.336(37)	760.840	2.67(45)			
			1317.983(046)	758.735	3.52(1.90)
1383.359(16)	722.878	6.28(46)			
1384.254(37)	722.411	2.63(46)			
1385.006(20)	722.018	4.81(46)			
1385.522(12)	721.750	8.48(46)			
1386.095(37)	721.451	2.62(46)			
1386.512(15)	721.235	6.45(46)			
1388.434(35)	720.236	2.78(46)			
1389.661(31)	719.600	3.18(46)			
1390.189(23)	719.327	4.21(46)			
1390.680(20)	719.073	4.82(46)			
1391.311(23)	718.746	4.22(46)			
1392.043(33)	718.369	2.97(46)			
1394.614(28)	717.044	3.45(46)			
1395.118(33)	716.785	2.94(46)			
2200.133(35)	454.518	2.83(51)			
			2213.161(046)	451.842	5.58(63)
			2213.695(052)	451.733	8.13(54)
			2214.635(062)	451.542	11.36(54)
			2214.985(055)	451.470	8.35(53)
			2407.200(015)	415.420	10.90(53)
2697.888(00)	370.660	2.49(42)			

3.7.1. New TESS observations

TESS observed the star in three sectors in the ultra-short cadence mode. By the Fourier analysis of the data set, we detected all three frequencies reported in the literature. Furthermore, we found a doublet in the Fourier transform at one of the frequencies, which may be the result of rotational frequency splitting. Table 8 summarises our findings together with the frequencies presented by Mukadam et al. (2004), while Fig. 7 shows the Fourier transform of the three-sector TESS observation.

3.8. HE 0532-5605

HE 0532-5605 (TIC 382303117, $\alpha_{2000} = 05^{\rm h}33^{\rm m}07^{\rm s}$, $\delta_{2000} = -56^{\rm d}03^{\rm m}53^{\rm s}$) is a known ZZ Ceti variable showing pulsation periods between about 400 and 1400 s (see the details and references in P01). Thanks to its location near the southern ecliptic pole, the former, 120-second measurements investigated in P01 covered 13 sectors of observations. However, we cannot detect any significant peaks neither by the analysing the individual sectors, nor by investigating the whole data set. What we found is a burst-like feature in the light curve obtained in the second half of the sector 1 observations. The duration of the presumed burst was about 24 h with an amplitude of nearly 20 per cent. We analysed both the first half of the sector 1 data set and the second half containing the burst-like event, respectively, and found that there are relatively large amplitude peaks emerged around 2530 μHz in the latter case, which can be in connection with the presumed outburst. However, we cannot detect such large amplitude event in the other sectors' light curves.

3.8.1. New TESS observations

The star was observed in ten sectors with the ultra-short cadence mode. Similarly to the former observations, we cannot detect any significant peaks in the Fourier transforms of the individual sectors or by the analysis of the whole data set. However, we investigated the 120-second cadence light curves as well, and found

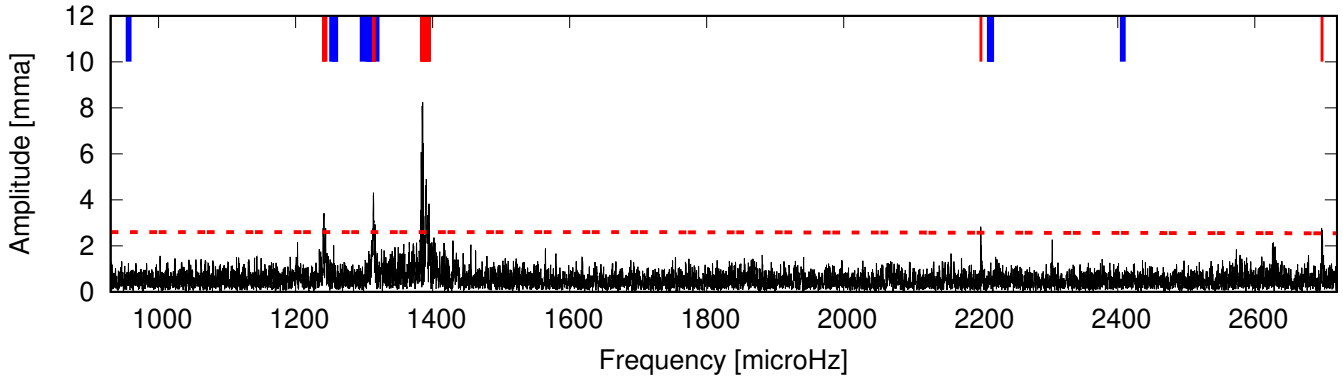

Fig. 5. Fourier transform of the ultra-short cadence mode TESS observations on MCT 0145-2211. For further explanation, see the caption of Fig. 2.

Table 7. This work: frequencies detected in the sector 38–39 data set of L 19-2. Yeates et al. (2005) presents frequencies and mode identification based on the results of a Whole Earth Telescope (Nather et al. 1990) campaign.

This work				Yeates et al. (2005)		
Frequency [μHz]	Period [s]	Amplitude [mma]		Frequency [μHz]	Period [s]	Amplitude [mma]
5178.857(12)	193.093	0.688(72)	f_1^{-1}	5179.362	193.074	0.973
5191.851(2)	192.610	3.627(72)	f_1^{0}	5191.795	192.612	5.535
			f_1^{+1}	5204.160	192.154	1.216
8789.057(8)	113.778	1.066(72)	f_2^{0}	8789.054	113.778	1.766
			f_2^{+2}	8828.619	113.268	0.271
8426.318(9)	118.676	0.892(72)	f_3^{-1}	8426.324	118.676	1.191
8437.439(8)	118.519	1.089(72)	f_3^{0}	8437.433	118.520	1.641
			f_3^{+1}	8448.580	118.363	0.339
			f_4^{0}	2855.785	350.166	0.918
			f_4^{+1}	2868.023	348.672	0.347
			$f_5^{-1?}$	6954.415	143.794	0.228
			f_5^{0}	6972.527	143.420	0.354
			f_5^{+1}	6991.176	143.038	0.341

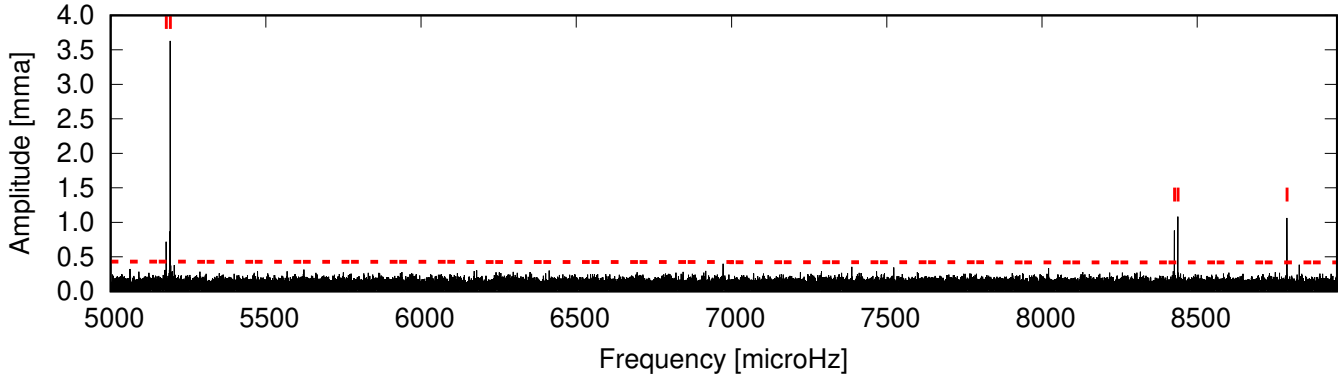

Fig. 6. Fourier transform of the ultra-short cadence TESS observations on L 19-2. Red lines denotes the significant frequencies we detected by the sector 38–39 measurements.

Table 8. Frequencies detected in the TESS data set of HS 1013+0321, and the periods found by Mukadam et al. (2004) for comparison.

This work				Mukadam et al. (2004)		
Frequency [μHz]	Period [s]	Amplitude [mma]		Frequency [μHz]	Period [s]	Amplitude [mma]
3701.931(2)	270.129	3.88(39)	f_1	3703.7	270.0	8.4
3922.823(1)	254.918	4.52(39)	f_2	3910.8	255.7	7.3
5121.767(2)	195.245	2.53(39)	$f_3^{-1,0?}$			
5128.417(2)	194.992	2.70(39)	$f_3^{0,-1?}$	5136.1	194.7	5.8

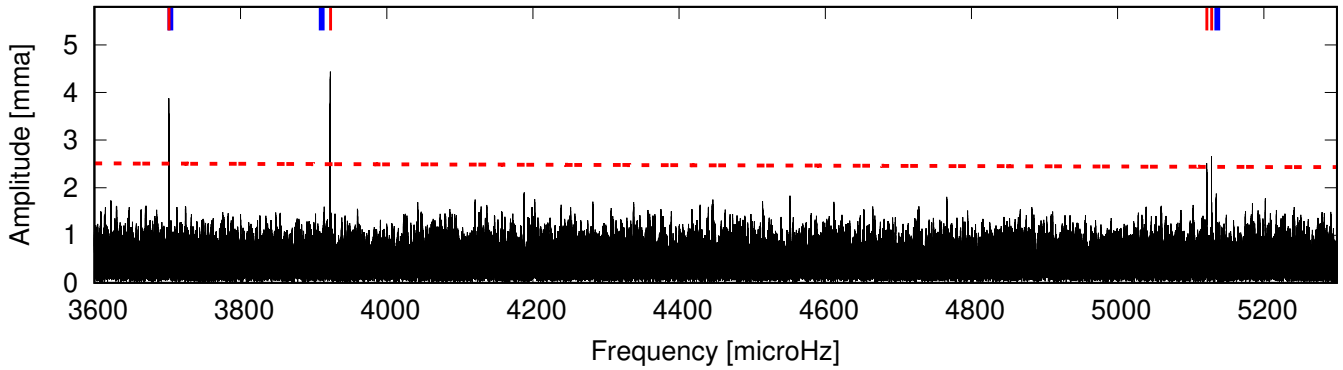

Fig. 7. Fourier transform of the ultrashort cadence mode TESS observations on HS 1013+0321. Red marks show the significant frequencies identified in this data, while blue marks show the location of pulsation components measured by Mukadam et al. (2004).

a very similar outburst-like feature in the sector 33 data like we saw in the previous TESS observations. That is, the event repeated, which strongly suggests that HE 0532-5605 is really a new outbursting cool DAV star. The flux increased by approximately 13 per cent during an interval of about 1 day. The amplitude is smaller than the sudden 20 per cent increase detected in sector 1, but the 1 day interval of the brightening phase is similar to the one observed previously. Figure 8 shows the corresponding part of the sector 33 light curve.

As in P01, we checked the frequency content of the two halves of the sector 33 light curve. The brightening occured during the first part of the observations, and as Fig. 9 reveals, we see relatively large amplitude peaks in the 2525–2545 μHz frequency domain in its Fourier transform. This phenomenon is in accordance with the former results. The largest amplitude peak can be found at 2530 μHz. All of this confirms that HE 0532-5605 is a DAV star, which shows outburst events from time to time.

3.9. WD J0925+0509

WD J0925+0509 (TIC 290653324, α_{2000} = $09^{h}25^{m}12^{s}$, δ_{2000} = $+05^{d}09^{m}33^{s}$) was classified as a NOV star in P01. We examined the new light curves, but did not find any periodic light variations at this time either.

3.9.1. New TESS observations

The star was observed in three sectors in ultra-short cadence mode. While we still did not find any sign of pulsational light variations, we identified an interesting brightening episode in the sector 46 light curve, similarly to the case of HE 0532-5605, shown in Fig 10. However, this was not intrinsic to the star. As it turns out, TESS coincidentally observed the minor planet (167578) 2004 BM_{72} crossing the aperture of this target, producing a several-hour-long brightening episode, rather similar in appearance to a weak outburst event. Obviously, the Fourier-spectrum of this light-curve segment also displays only noise.

4. Summary and conclusions

We focused on the results of the ultra-short cadence (20 s) mode TESS observations of nine white dwarf stars known as ZZ Ceti variables. These stars were presented also in P01, but in that case the shortest cadence mode available was 120 s only. The new TESS observations allow us to determine the pulsation modes without the Nyquist ambiguities of the 120 s measurements, and to compare the frequency contents between the different observational cycles. Note that we investigated the measurements on 18 previously known ZZ Ceti stars in P01, however, more than half of them did not show periodic light variations in the TESS observations. We explained this as the results mainly due to the faintness of these targets, in combination with the crowding of the large TESS pixels.

Considering the new observations presented in this paper, we found significant pulsational frequencies in seven stars. Additionally, we detected one-one brightening episodes in the light curves of two targets. In the case of the first one, HE 0532-5605, we detected a similar brightening phase as earlier, described in P01, that is, the phenomenon is recurring, implying that HE 0532-5605 is most probably a new outbursting ZZ Ceti star. However, the observed brightening of the other star, WD J0925+0509, was extrinsic, caused by a passing minor planet crossing the photometric aperture of the star in the TESS images.

Finally, we briefly summarise our results on the different stars showing pulsations based on the new ultra-short cadence TESS observations:

Ross 548: we can clearly detect the four highest-amplitude frequencies by the ultra-short cadence data, without the Nyquist alias ambiguities of the 120 s cadence observations.

EC 23487-2424: the dominant frequency is different from the one detected in the previous TESS data. Some of the peaks seem to be unstable in amplitude/frequency/phase, producing additional peaks around them.

BPM 31594: we found practically all the frequencies detected previously, and several additional frequencies, too.

BPM 30551: only new frequencies were detected, although one of them very near to another detected in the first TESS data set in P01.

MCT 0145-2211: new frequencies only, none of the old ones appeared in the new TESS data, almost as we observed a different star.

L 19-2: one already known frequency, and four additional frequencies in the 20 s cadence data.

HS 1013+0321: the first TESS data set did not show pulsational light variations, while in the new TESS data, we detected all three frequencies reported earlier in the literature. We also detected a new peak, which appears to be the result of rotational frequency splitting.

The newly detected frequencies will impose stronger constraints on future asteroseismological modellings. We always

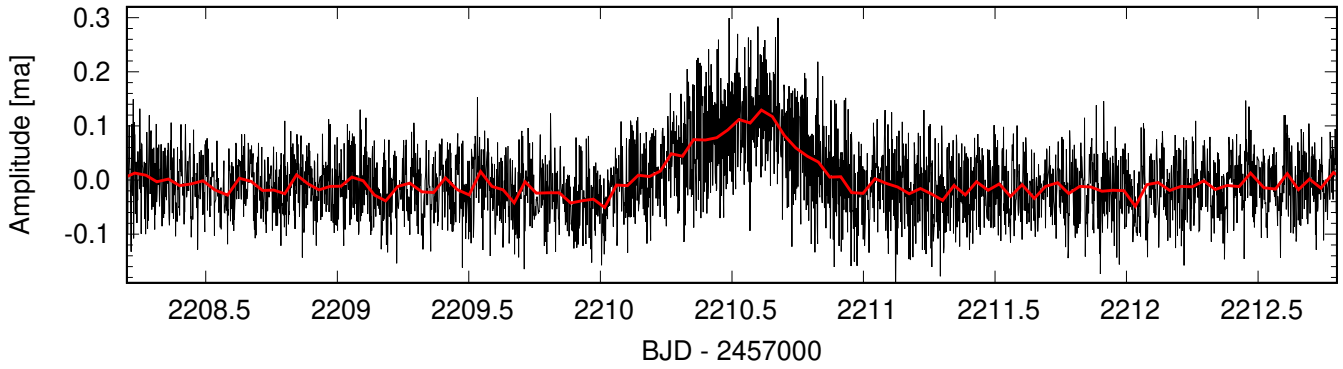

Fig. 8. HE 0532-5605: portion of the light curve obtained by TESS during the section 33 120-second cadence mode observations (black line). The red line shows this light curve as binned, with a bin size of 30 points. The about 13 per cent flux emergence is obvious, and it takes about 1 day.

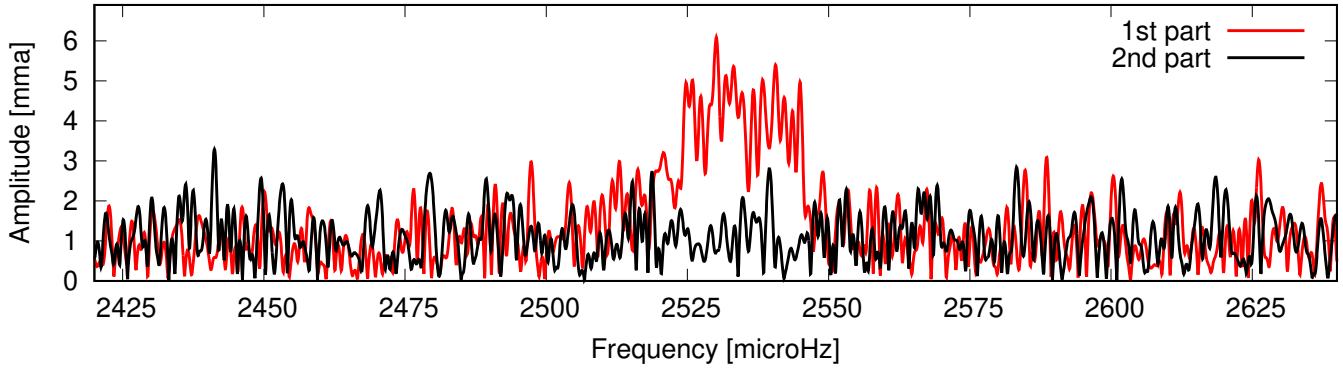

Fig. 9. HE 0532-5605: red and black lines denote the Fourier transforms of the first and second halves of the light curve obtained in sector 33 and in 120-second cadence mode, respectively. The brightening effect in the light curve emerged during the first half of the observations.

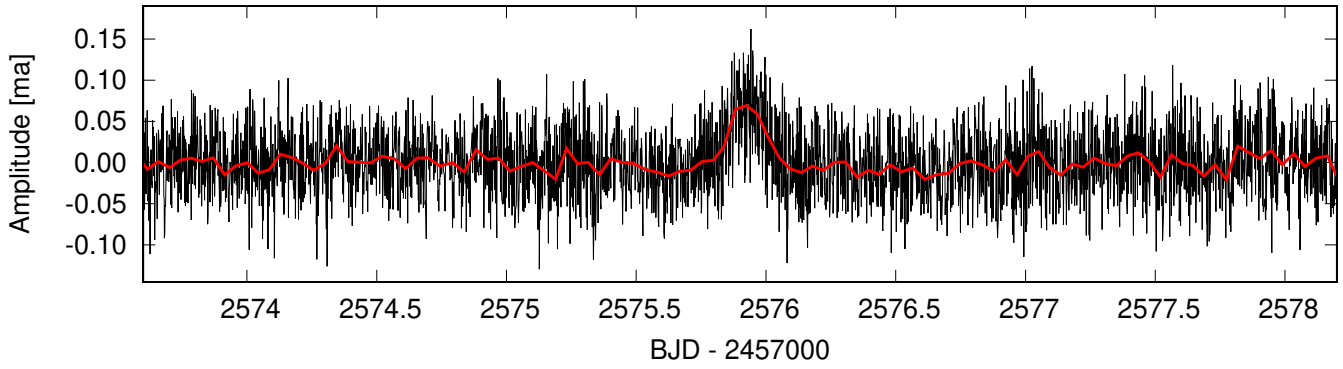

Fig. 10. WD J0925+0509: portion of the light curve obtained by TESS during the section 46 120-second cadence mode observations (black line). The red line shows this light curve as binned, with a bin size of 30 points. The maximum of the flux emergence is about 7 per cent, and the phenomenon takes about 0.5 day.

have to keep in mind that the ultimate goal of our efforts of detecting as many pulsation modes as we possibly can, is learning more about the internal structure of the target stars and their non-pulsating counterparts, and about the dynamical processes operating inside the pulsators. The new, ultra-short cadence mode observations showed their high value in studying the white dwarf variables, and the continuation of these measurements could be extremely valuable for the white dwarf community.

Acknowledgements. ZsB and ÁS acknowledge the financial support of the Lendület Program of the Hungarian Academy of Sciences, projects No. LP2018-7/2022, and LP2012-31. This research was supported by the KKP-137523 'SeismoLab' Élvonal grant of the Hungarian Research, Development and Innovation Office (NKFIH). ZsB acknowledges the support by the János Bolyai Research Scholarship of the Hungarian Academy of Sciences. This paper includes data collected with the TESS mission, obtained from the MAST data archive at the Space Telescope Science Institute (STScI). Funding for the TESS mission is provided by the NASA Explorer Program. STScI is operated by the Association of Universities for Research in Astronomy, Inc., under NASA contract NAS 5–26555.

References

Althaus, L. G., Córsico, A. H., Isern, J., & García-Berro, E. 2010, A&A Rev., 18, 471

Bell, K. J., Córsico, A. H., Bischoff-Kim, A., et al. 2019, A&A, 632, A42

Bell, K. J., Hermes, J. J., Montgomery, M. H., et al. 2017, in Astronomical Society of the Pacific Conference Series, Vol. 509, 20th European White Dwarf Workshop, ed. P.-E. Tremblay, B. Gaensicke, & T. Marsh, 303
Bognár, Z., Kawaler, S. D., Bell, K. J., et al. 2020, A&A, 638, A82
Brickhill, A. J. 1991, MNRAS, 251, 673
Charpinet, S., Brassard, P., Fontaine, G., et al. 2019, A&A, 632, A90
Córsico, A. H. 2020, Frontiers in Astronomy and Space Sciences, 7, 47
Córsico, A. H., Althaus, L. G., Miller Bertolami, M. M., & Kepler, S. O. 2019, A&A Rev., 27, 7
Dolez, N. & Vauclair, G. 1981, A&A, 102, 375
Fontaine, G. & Brassard, P. 2008, PASP, 120, 1043
Giammichele, N., Fontaine, G., Bergeron, P., et al. 2015, ApJ, 815, 56
Goldreich, P. & Wu, Y. 1999, ApJ, 511, 904
Hermes, J. J., Gänsicke, B. T., Kawaler, S. D., et al. 2017, ApJS, 232, 23
Jenkins, J. M., Twicken, J. D., McCauliff, S., et al. 2016, in Proc. SPIE, Vol. 9913, Software and Cyberinfrastructure for Astronomy IV, 99133E
Mukadam, A. S., Mullally, F., Nather, R. E., et al. 2004, ApJ, 607, 982
Nather, R. E., Winget, D. E., Clemens, J. C., Hansen, C. J., & Hine, B. P. 1990, ApJ, 361, 309
Ricker, G. R., Winn, J. N., Vanderspek, R., et al. 2015, Journal of Astronomical Telescopes, Instruments, and Systems, 1, 014003
Romero, A. D., Kepler, S. O., Hermes, J. J., et al. 2022, MNRAS, 511, 1574
Sodor, A. 2012, Konkoly Observatory Occasional Technical Notes, 15, 1
Stobie, R. S., Chen, A., O'Donoghue, D., & Kilkenny, D. 1993, MNRAS, 263, L13
Winget, D. E. & Kepler, S. O. 2008, ARA&A, 46, 157
Winget, D. E., van Horn, H. M., Tassoul, M., et al. 1982, ApJ, 252, L65
Yeates, C. M., Clemens, J. C., Thompson, S. E., & Mullally, F. 2005, ApJ, 635, 1239
Zong, W., Charpinet, S., Vauclair, G., Giammichele, N., & Van Grootel, V. 2016, A&A, 585, A22